1-1-2014

Dynamic Modeling and Analysis of Generalized Power Flow Controller

B. Vyakaranam
Cleveland State University

F. E. Villaseca

Publisher's Statement

NOTICE: this is the author's version of a work that was accepted for publication in Electric Power Systems Research. Changes resulting from the publishing process, such as peer review, editing, corrections, structural formatting, and other quality control mechanisms may not be reflected in this document. Changes may have been made to this work since it was submitted for publication. A definitive version was subsequently published in Electric Power Systems Research, 106, , (01-01-2014); 10.1016/j.epsr.2013.07.010

Dynamic modeling and analysis of generalized unified power flow controller

B. Vyakaranam*, F.E. Villaseca

Department of Electrical and Computer Engineering, Cleveland State University, OH, USA

1. Introduction

Over the last few decades, the use of semiconductor devices in large-scale power systems has spread around the world due to the increased ratings of these devices, and resulting in an area of academic study we now call high-power electronics [1,2]. These devices are used to improve the electrical and economic performance of power transmission systems, which the electric utilities companies use to deliver electricity to their customers [3]. But since they are nonlinear devices, they produce undesirable distortions in the voltage and current waveforms in the circuits to which they are connected. These distortions also result in the presence of undesirable harmonics [4].

The study of the harmonic content of distorted, but periodic, waveforms via the simulation of time-domain (TD) models require long simulation run times. This is a consequence of the need to let the transients die out and to allow sufficient time, under steady-state conditions, for the accurate calculation of the harmonics via the fast Fourier transform (FFT) [5–9]. Electromagnetic transients' simulations tools such as PSCAD/EMTDC can be used to calculate transients as a function of time. To compute the harmonic content during the corresponding period of interest, a post-processing routine can then be used. Fox example, windowed fast Fourier Transform (WFFT) method has been used for the calculation of harmonic information of a signal. However, this method has some drawbacks such as leakage picket-fence, aliasing, and edge effect [10]. Additionally, this method is dependent on the size of the window to achieve accuracy in results. However, adjusting the size of this window is not a small procedure. Hence, keeping in mind these drawbacks, it is difficult to accurately assess power quality. The time-domain methods with WFFT achieve harmonic behavior of the system under stationary conditions. However, these methods lose their accuracy during time-varying conditions [10]. Therefore, it is not possible to capture the accurate harmonic response of the system using these methods with WFFT during fast disturbances.

An alternative methodology has been proposed, which models the systems in the harmonic-domain (HD) rather than in the time domain, thus producing models for the steady-state simulation [7]. This has been demonstrated by its application to high-voltage DC (HVDC) transmission systems [11–14], and in flexible AC transmission systems (FACTS) such as fixed capacitor-thyristor controlled reactor (FC-TCR) [15,16], thyristor-controlled reactor (TCR) [17], thyristor-controlled switched capacitors (TCSC) [15], static compensators (STATCOM) [18,19], static synchronous series compensators (SSSC) [20], and unified power flow controllers (UPFC) [14,21,22].

The procedure in [39] referred to as phasor dynamics, for the first time, is to give prominence to the time-varying nature of the signals in phasor description. Dynamic phasor models incorporate the relatively large Fourier coefficients [39] which in most cases is the DC

* Corresponding author. Tel.: +1 216 577 0675.
E-mail address: bharat.csu@gmail.com (B. Vyakaranam).

component. This technique is based on the generalized averaging method and it has been applied to obtain FACTS controller models [40]. In [39] the paper was focused on the representation of the DC and fundamental frequency components. However, additional harmonic terms can significantly improve the efficacy of models. It was recommended that effects of important harmonics should be included in the models [40].

Recently, a new methodology, the dynamic harmonic domain (DHD) technique, which is an extension of the theory of dynamic phasors to provide a dynamic, harmonic frame of reference, has been proposed [23]. This allows for the determination of the harmonic content of distorted waveforms, not only in the steady state, but also during transients. The proposed DHD methodology has been demonstrated by its application to the study of the dynamic behavior of harmonics in HVDC [14], STATCOM [23], TCR [24], SVC [25,26], SSSC [25,26] and UPFC [25,26] systems, and has shown that DHD models have none of the disadvantages associated with WFFT and therefore it is a possible method to be used for the accurate assessment of power quality [23]. Recently, the DHD modeling has been successfully applied for several applications in transmission and distribution systems [27–32]. The DHD modeling approach can also be applied to multi-phase, multi-machine systems. This is explained as follows: In [9,18] the multi-pulse STATCOM was modeled using HD and was simulated using multi-phase switching functions in order to understand the reaction of these controllers to various switching functions and study their influence on power quality indices under steady and disturbance conditions. DHD methodology is applicable for all the power electronics controller HD models developed in the open literature [9].

This paper presents the DHD modeling of a much more complex controller, the generalized unified power flow controller (GUPFC) [33], which is a multi-line voltage-source controller and one of the newest additions to the set of FACTS controllers. A simulation of the proposed model allows for the assessment of power quality by the calculation of power quality indices.

The paper is organized as follows: in Section 2, the basic theory of the dynamic harmonic-domain methodology is presented. Section 3, the main contribution of this study, presents the DHD modeling of the GUPFC. Numerical results are presented and discussed in Section 4. It also includes a validation of the model results by a comparison to time domain results.

2. Dynamic harmonic domain

The following development of the dynamic harmonic domain method is adapted from [23,34,35]. A continuous, periodic function $x(t)$ with $t \in (-\infty, \infty)$ and period T may be represented to any degree of accuracy by the time-dependent complex Fourier series given by [36].

$$x(t) = \sum_{n=-\infty}^{\infty} X_n(t) e^{jn\omega_0 t} \tag{1}$$

where $\omega_0 = 2\pi/T$. Note that the complex Fourier coefficients $X_n(t)$ depend on time in the following manner. At any time t, consider a time window of length T just prior to t, namely the interval $[t-T, t]$ Then the Fourier coefficients that are assigned to t are taken to be

$$X_n(t) = \frac{1}{T} \int_{t-T}^{t} x(\tau) e^{-jn\omega_0 \tau} d\tau \tag{2}$$

The complex coefficients in (2) are referred to as *dynamic phasors* [34]. This representation of the signal $x(t)$ is the fundamental concept which underlies the DHD method. Eq. (2) gives the time-evolution of the complex Fourier coefficients as a window of length T is translated along the waveform $x(t)$.

For numerical calculations the infinite sum in (1) can be limited to a finite number of harmonics, say $n \in [-h, h]$. Then $x(t)$ may be approximated by

$$x(t) \approx \sum_{n=-h}^{h} X_n(t) e^{jn\omega_0 t} \tag{3}$$

In this case, (3) may be represented in matrix notation by

$$x(t) = \mathbf{G}^{\mathrm{T}}(t)\mathbf{X}(t) \tag{4}$$

where

$$\begin{aligned} \mathbf{G}(t) &= \begin{bmatrix} e^{-jh\omega_0 t} & \cdots & e^{-j\omega_0 t} & 1 & e^{j\omega_0 t} & \cdots & e^{jh\omega_0 t} \end{bmatrix}^T \text{and} \\ \mathbf{X}(t) &= \begin{bmatrix} X_{-h}(t) & \cdots & X_{-1}(t) & X_0(t) & X_1(t) & \cdots & X_h(t) \end{bmatrix}^T \end{aligned} \tag{5}$$

The vector $\mathbf{G}(t)$ is made up of the first $2h+1$ orthogonal basis elements in the complex Fourier series representation of $x(t)$ and $\mathbf{X}(t)$ is the vector whose components are the harmonic coefficients of $x(t)$

State-space models can be expressed in the DHD as follows. Consider the linear time-periodic (LTP) system

$$\begin{aligned} \dot{x}(t) &= a(t)x(t) + b(t)u(t) \\ y(t) &= c(t)x(t) + e(t)u(t) \end{aligned} \tag{6}$$

where all functions are assumed to have period T.

In order to transform (6) into the harmonic domain, some preliminary results are needed. Differentiating (4) gives

$$\dot{x}(t) = \mathbf{G}^T(t)\dot{\mathbf{X}}(t) + \dot{\mathbf{G}}^T(t)\mathbf{X}(t) \tag{7}$$

The derivative of the basis vector $\mathbf{G}(t)$ can be expressed as

$$\dot{\mathbf{G}}(t) = \mathbf{D}(jh\omega_0)\mathbf{G}(t) \tag{8}$$

where $\mathbf{D}(jh\omega_0)$ is the matrix of differentiation defined by

$$D(jh\omega_0) = \begin{bmatrix} -jh\omega_0 & 0 & 0 & 0 & 0 & 0 & 0 \\ 0 & \ddots & 0 & 0 & 0 & 0 & 0 \\ 0 & 0 & -j\omega_0 & 0 & 0 & 0 & 0 \\ 0 & 0 & 0 & 0 & 0 & 0 & 0 \\ 0 & 0 & 0 & 0 & j\omega_0 & 0 & 0 \\ 0 & 0 & 0 & 0 & 0 & \ddots & 0 \\ 0 & 0 & 0 & 0 & 0 & 0 & jh\omega_0 \end{bmatrix} \tag{9}$$

Transposing (8) gives

$$\dot{\mathbf{G}}^T(t) = \mathbf{G}^T(t)\mathbf{D}(jh\omega_0) \tag{10}$$

and substituting this result into (7) gives

$$\dot{x}(t) = \mathbf{G}^T(t)\dot{\mathbf{X}}(t) + \mathbf{G}^T(t)\mathbf{D}(jh\omega_0)\mathbf{X}(t) \tag{11}$$

Next, the product of two periodic functions such as $a(t)x(t)$ is transformed as follows. Expand $x(t)$ as into its finite Fourier series approximation as

$$\begin{aligned} x(t) &= X_{-h}e^{-jh\omega_0 t} + \cdots + X_{-1}e^{-j\omega_0 t} + X_0 + X_1 e^{j\omega_0 t} + \cdots + X_h e^{jh\omega_0 t} \\ &= \mathbf{G}^T(t)\mathbf{X} \end{aligned} \tag{12}$$

where

$$\mathbf{X} = \begin{bmatrix} X_{-h}(t) & \cdots & X_{-1}(t) & X_0(t) & X_1(t) & \cdots & X_h(t) \end{bmatrix}^T \tag{13}$$

Similarly,

$$\begin{aligned} a(t) &= A_{-h}e^{-jh\omega_0 t} + \cdots + A_{-1}e^{-j\omega_0 t} + A_0 + A_1 e^{j\omega_0 t} + \cdots + A_h e^{jh\omega_0 t} \\ &= \mathbf{G}^T(t)\mathbf{A} \end{aligned} \tag{14}$$

Therefore,

$$a(t)x(t) = \mathbf{G}^{\mathrm{T}}(t)\mathbf{A}\mathbf{G}^{\mathrm{T}}(t)\mathbf{X} = \mathbf{G}^{\mathrm{T}}(t)\mathbf{A}\mathbf{X} \tag{15}$$

where $\mathbf{A}$ is the Toeplitz matrix given by

$$\mathbf{A} = \begin{bmatrix} A_0 & A_{-1} & \cdots & A_{-h} & & & \\ A_1 & \ddots & \ddots & \ddots & \ddots & & \\ \vdots & \ddots & A_0 & A_{-1} & \ddots & \ddots & \\ A_h & \ddots & A_1 & A_0 & A_{-1} & \ddots & A_{-h} \\ & \ddots & \ddots & A_1 & A_0 & \ddots & \vdots \\ & & \ddots & \ddots & \ddots & \ddots & A_{-1} \\ & & & A_h & \cdots & A_1 & A_0 \end{bmatrix} \tag{16}$$

Similar constructions are employed to transform the other products of periodic functions in (6) to give

$$b(t)u(t) = \mathbf{G}^{\mathrm{T}}(t)\mathbf{B}\mathbf{U};\ c(t)x(t) = \mathbf{G}^T(t)\mathbf{C}\mathbf{X};\ e(t)u(t) = \mathbf{G}^T(t)\mathbf{E}\mathbf{U} \tag{17}$$

Substituting the various harmonic domain expressions into (6) gives

$$\begin{aligned} \mathbf{G}^{\mathrm{T}}\dot{\mathbf{X}} + \mathbf{G}^{\mathrm{T}}\mathbf{D}(jh\omega_0)\mathbf{X} &= \mathbf{G}^{\mathrm{T}}\mathbf{A}\mathbf{X} + \mathbf{G}^{\mathrm{T}}\mathbf{B}\mathbf{U} \\ \mathbf{G}^{\mathrm{T}}\mathbf{Y} &= \mathbf{G}^{\mathrm{T}}\mathbf{C}\mathbf{X} + \mathbf{G}^{\mathrm{T}}\mathbf{E}\mathbf{U} \end{aligned} \tag{18}$$

Finally, rearranging and canceling the common vectors of basis elements $\mathbf{G}^{\mathrm{T}}$ gives the compact representation of the system in the DHD:

$$\begin{aligned} \dot{\mathbf{X}} &= (\mathrm{A} - \mathrm{D}(jh\omega_0))\mathbf{X} + \mathbf{B}\mathbf{U} \\ \mathbf{Y} &= \mathbf{C}\mathbf{X} + \mathbf{E}\mathbf{U} \end{aligned} \tag{19}$$

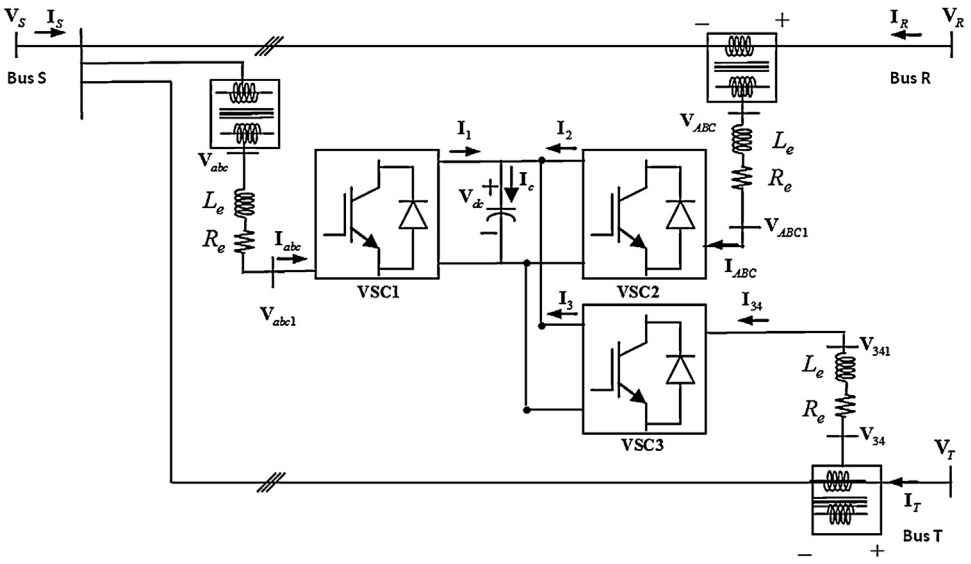

Fig. 1. Generalized unified power flow controller.

The full harmonic dynamic behavior of variables $x(t)$ and $y(t)$ can be obtained by solving the equations in(19). These equations are the key to the DHD methodology.

3. Generalized unified power flow controller

The development of the generalized unified power flow controller model will now be presented. The GUPFC consists of three voltage source converters, VSC 1, VSC 2, and VSC 3 [33] as shown in Fig. 1. Here, one converter is connected in shunt and the other two in series with two transmission lines. The shunt controller injects three-phase current and the series controllers inject three-phase voltages into the AC system. These converters are connected back-to-back across a common DC link, a storage capacitor, thus facilitating real power transfer. The benefit of this design is that these three converters can independently generate or absorb reactive power.

3.1. Dynamic harmonic domain model of the GUPFC

The derivation of the proposed GUPFC DHD model, also not currently available in the literature, is now presented.

The three-phase voltages and currents on the AC sides of the GUPFC Fig. 1 are $\mathbf{v}_{abc1}(t), \mathbf{v}_{ABC1}(t), \mathbf{v}_{341}(t), \mathbf{i}_{abc}(t), \mathbf{i}_{ABC}(t)$ and $\mathbf{i}_{34}(t)$, respectively, and can be expressed in terms of DC-side voltage $\mathbf{v}_{dc}(t)$, DC-side current $i_1(t)$, $i_2(t)$, and $i_3(t)$, and the switching functions as

$$\mathbf{v}_{abc1}(t) = \mathbf{p}_{s1}(t)v_{dc}(t); \mathbf{v}_{ABC1}(t) = \mathbf{p}_{s2}(t)v_{dc}(t); \mathbf{v}_{341}(t) = \mathbf{p}_{s3}(t)v_{dc}(t) \tag{20}$$

$$i_1(t) = \mathbf{q}_{s1}(t)\mathbf{i}_{abc}(t); i_2(t) = \mathbf{q}_{s2}(t)\mathbf{i}_{ABC}(t); i_3(t) = \mathbf{q}_{s3}(t)\mathbf{i}_{34}(t) \tag{21}$$

where $\mathbf{p}_{s1}(t)$, $\mathbf{p}_{s2}(t)$, $\mathbf{p}_{s3}(t)$, $\mathbf{q}_{s1}(t)$, $\mathbf{q}_{s2}(t)$ and $\mathbf{q}_{s3}(t)$ are transformation vectors, given by

$$\begin{aligned} \mathbf{p}_{s1}(t) &= \begin{bmatrix} s_{ab1}(t) \\ s_{bc1}(t) \\ s_{ca1}(t) \end{bmatrix}; \ \mathbf{p}_{s2}(t) = \begin{bmatrix} s_{ab2}(t) \\ s_{bc2}(t) \\ s_{ca2}(t) \end{bmatrix}; \ \mathbf{p}_{s3}(t) = \begin{bmatrix} s_{ab3}(t) \\ s_{bc3}(t) \\ s_{ca3}(t) \end{bmatrix}; \ \mathbf{q}_{s1}(t) = \begin{bmatrix} s_{ab1}(t) \\ s_{bc1}(t) \\ s_{ca1}(t) \end{bmatrix}^T \\ \mathbf{q}_{s2}(t) &= [\, s_{ab2}(t) \quad s_{bc2}(t) \quad s_{ca2}(t)\,]; \ \mathbf{q}_{s3}(t) = [\, s_{ab3}(t) \quad s_{bc3}(t) \quad s_{ca3}(t)\,] \end{aligned} \tag{22}$$

$s_{ab1}(t)$, $s_{bc1}(t)$, and $s_{ca1}(t)$ are the switching functions of VSC 1, $s_{ab2}(t)$, $s_{bc2}(t)$, and $s_{ca2}(t)$ are for VSC 2 and $s_{ab3}(t)$, $s_{bc3}(t)$, and $s_{ca3}(t)$ are for VSC 3. Fig. 2 shows a conventional three-phase voltage source converter that consists of six anti-parallel diodes D1–D6, and six switches S1–S6 [18]. The number for each diode and switch indicates its order on being turned on. Total equivalent impedance, Z_e indicates the equivalent resistance and reactance of the transmission line as well as the star-delta transformer. The line currents of the primary side of the transformer are proportional to line currents of the secondary side of the transformer. There is a phase shift of 120° between the three converter legs that are controlled.

The following state equation describes the circuit dynamics on the DC-side of the GUPFC:

$$\frac{dv_{dc}(t)}{dt} = \frac{1}{C}(i_1(t) + i_2(t) + i_3(t)) \tag{23}$$

Substitution of Eq. (21) into (23) yields

$$\frac{dv_{dc}(t)}{dt} = \frac{1}{C}(\mathbf{q}_{s1}(t)\mathbf{i}_{abc}(t) + \mathbf{q}_{s2}(t)\mathbf{i}_{ABC}(t) + \mathbf{q}_{s3}(t)\mathbf{i}_{34}(t)) \tag{24}$$

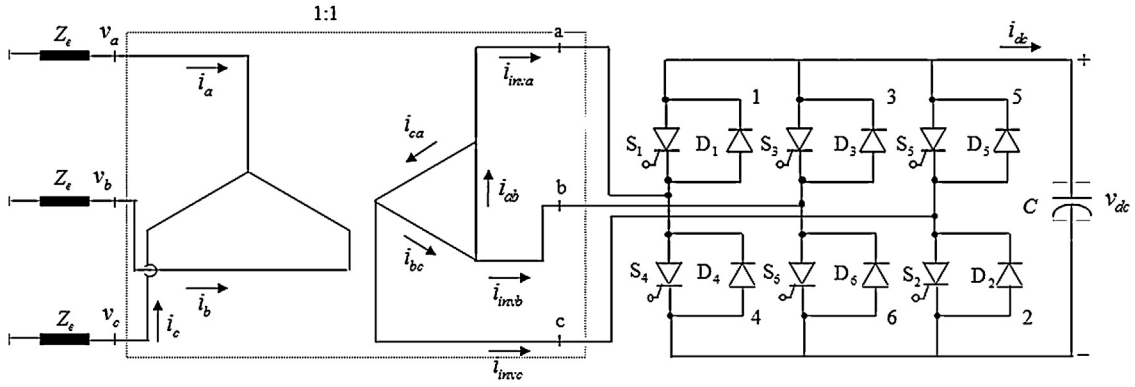

Fig. 2. Three-phase voltage source converter.

The voltage drop across the equivalent three-phase impedance of the transformer connected to the VSC 1 is

$$R_e\mathbf{i}_{abc}(t)+L_e\frac{d\mathbf{i}_{abc}(t)}{dt}=\mathbf{v}_{abc}(t)-\mathbf{v}_{abc1}(t)$$
$$\frac{d\mathbf{i}_{abc}(t)}{dt}=-\frac{R_e}{L_e}\mathbf{i}_{abc}(t)+\frac{\mathbf{v}_{abc}(t)-\mathbf{v}_{abc1}(t)}{L_e} \tag{25}$$

Similarly for VSC 2 is

$$R_e\mathbf{i}_{ABC}(t)+L_e\frac{d\mathbf{i}_{ABC}(t)}{dt}=\mathbf{v}_{ABC}(t)-\mathbf{v}_{ABC1}(t)$$
$$\frac{d\mathbf{i}_{ABC}(t)}{dt}=-\frac{R_e}{L_e}\mathbf{i}_{ABC}(t)+\frac{\mathbf{v}_{ABC}(t)-\mathbf{v}_{ABC1}(t)}{L_e} \tag{26}$$

For VSC 3 is

$$R_e\mathbf{i}_{34}(t)+L_e\frac{d\mathbf{i}_{34}(t)}{dt}=\mathbf{v}_{34}(t)-\mathbf{v}_{341}(t)$$
$$\frac{d\mathbf{i}_{34}(t)}{dt}=-\frac{R_e}{L_e}\mathbf{i}_{34}(t)+\frac{\mathbf{v}_{34}(t)-\mathbf{v}_{341}(t)}{L_e} \tag{27}$$

Substitution of Eq. (20) into (25), (26), and (27) yields

$$\frac{d\mathbf{i}_{abc}(t)}{dt}=-\frac{R_e}{L_e}\mathbf{i}_{abc}(t)+\frac{1}{L_e}(\mathbf{v}_{ABC}(t)-\mathbf{p}_{s1}(t)v_{dc}(t)) \tag{28}$$

$$\frac{d\mathbf{i}_{ABC}(t)}{dt}=-\frac{R_e}{L_e}\mathbf{i}_{ABC}(t)+\frac{1}{L_e}(\mathbf{v}_{ABC}(t)-\mathbf{p}_{s2}(t)v_{dc}(t)) \tag{29}$$

$$\frac{d\mathbf{i}_{34}(t)}{dt}=-\frac{R_e}{L_e}\mathbf{i}_{34}(t)+\frac{1}{L_e}(\mathbf{v}_{34}(t)-\mathbf{p}_{s3}(t)\mathbf{v}_{dc}(t)) \tag{30}$$

The boundary conditions of the GUPFC are

$$\mathbf{i}_{abc}(t)=\mathbf{i}_R(t)+\mathbf{i}_S(t);\ \mathbf{i}_{ABC}(t)=\mathbf{i}_R(t);\ \mathbf{i}_{34}(t)=\mathbf{i}_T(t)$$
$$\mathbf{v}_{abc}(t)=\mathbf{v}_S(t);\ \mathbf{v}_{ABC}(t)=\mathbf{v}_R(t)-\mathbf{v}_S(t);\ \mathbf{v}_{34}(t)=\mathbf{v}_T(t)-\mathbf{v}_S(t) \tag{31}$$

Substitution of (31) into (24), (28), (29), and (30) yields

$$\frac{dv_{dc}(t)}{dt}=\frac{1}{C}(\mathbf{q}_{s1}(t)\mathbf{i}_S(t)+(\mathbf{q}_{s1}(t)+\mathbf{q}_{s2}(t)\mathbf{i}_R(t)+\mathbf{q}_{s3}(t)\mathbf{i}_T(t)) \tag{32}$$

$$\frac{d(\mathbf{i}_R(t)+\mathbf{i}_S(t))}{dt}=-\frac{R_e}{L_e}(\mathbf{i}_R(t)+\mathbf{i}_S(t))+\frac{1}{L_e}(\mathbf{v}_S(t)-\mathbf{p}_{s1}(t)v_{dc}(t)) \tag{33}$$

$$\frac{d\mathbf{i}_R(t)}{dt}=-\frac{R_e}{L_e}\mathbf{i}_R(t)+\frac{1}{L_e}(\mathbf{v}_R(t)-\mathbf{v}_S(t)-\mathbf{p}_{s2}(t)v_{dc}(t)) \tag{34}$$

$$\frac{d\mathbf{i}_T(t)}{dt}=-\frac{R_e}{L_e}\mathbf{i}_T(t)+\frac{1}{L_e}(\mathbf{v}_T(t)-\mathbf{v}_S(t)-\mathbf{p}_{s3}(t)v_{dc}(t)) \tag{35}$$

Substituting (34) into (33) gives

$$\frac{d\mathbf{i}_S(t)}{dt}=-\frac{R_e}{L_e}\mathbf{i}_S(t)+\frac{2\mathbf{v}_S(t)}{L_e}-\frac{\mathbf{v}_R(t)}{L_e}+\frac{\mathbf{v}_{dc}(t)}{L_e}(\mathbf{p}_{s2}(t)-\mathbf{p}_{s1}(t)) \tag{36}$$

The state Eqs. (32), (34) (35) and (36) of the GUPFC are

$$\begin{bmatrix} \frac{d\mathbf{i}_R(t)}{dt} \\ \frac{d\mathbf{i}_S(t)}{dt} \\ \frac{d\mathbf{i}_T(t)}{dt} \\ \frac{dv_{dc}(t)}{dt} \end{bmatrix} = \begin{bmatrix} -\frac{R_e}{L_e} & 0 & 0 & -\frac{\mathbf{p}_{s2}(t)}{L_e} \\ 0 & -\frac{R_e}{L_e} & 0 & -\left(\frac{\mathbf{p}_{s1}(t)-\mathbf{p}_{s2}(t)}{L_e}\right) \\ 0 & 0 & -\frac{R_e}{L_e} & -\frac{\mathbf{p}_{s3}(t)}{L_e} \\ \frac{\mathbf{q}_{s1}(t)+\mathbf{q}_{s2}(t)}{C} & \frac{\mathbf{q}_{s1}(t)}{C} & \frac{\mathbf{q}_{s3}(t)}{C} & 0 \end{bmatrix} \begin{bmatrix} \mathbf{i}_R(t) \\ \mathbf{i}_S(t) \\ \mathbf{i}_T(t) \\ v_{dc}(t) \end{bmatrix} + \frac{1}{L_e} \begin{bmatrix} 1 & -1 & 0 & 0 \\ -1 & 2 & 0 & 0 \\ 0 & -1 & 1 & 0 \\ 0 & 0 & 0 & 0 \end{bmatrix} \begin{bmatrix} \mathbf{v}_R(t) \\ \mathbf{v}_S(t) \\ \mathbf{v}_T(t) \\ 0 \end{bmatrix} \tag{37}$$

The state-space GUPFC model in (37) can be transformed into a DHD representation by making use of the procedure presented in Section 3.2. The resulting DHD model is given by

$$\begin{bmatrix} \dot{\mathbf{I}}_R(t) \\ \dot{\mathbf{I}}_S(t) \\ \dot{\mathbf{I}}_T(t) \\ \dot{\mathbf{V}}_{dc}(t) \end{bmatrix} = \mathbf{G}_U(t) \begin{bmatrix} \mathbf{I}_R(t) \\ \mathbf{I}_S(t) \\ \mathbf{I}_T(t) \\ \mathbf{V}_{dc}(t) \end{bmatrix} + \frac{1}{L_e} \begin{bmatrix} \mathbf{U}_1 & -\mathbf{U}_1 & \mathbf{O}_4 & O_2 \\ -\mathbf{U}_1 & 2\mathbf{U}_1 & \mathbf{O}_4 & O_2 \\ \mathbf{O}_4 & -\mathbf{U}_1 & \mathbf{U}_1 & O_2 \\ O_1 & O_1 & O_1 & O_3 \end{bmatrix} \begin{bmatrix} \mathbf{V}_R(t) \\ \mathbf{V}_S(t) \\ \mathbf{V}_T(t) \\ O \end{bmatrix} \tag{38}$$

where

$$\mathbf{G}_U(t) = \begin{bmatrix} -\frac{R_e}{L_e}\mathbf{U}_1 - \mathbf{D}(jh\omega_0) & \mathbf{O}_4 & \mathbf{O}_4 & -\frac{1}{L_e}\mathbf{P}_{S2} \\ \mathbf{O}_4 & -\frac{R_e}{L_e}\mathbf{U}_1 - \mathbf{D}(jh\omega_0) & \mathbf{O}_4 & -\left(\frac{\mathbf{P}_{S1}-\mathbf{P}_{S2}}{L_e}\right) \\ \mathbf{O}_4 & \mathbf{O}_4 & -\frac{R_e}{L_e}\mathbf{U}_1 - \mathbf{D}(jh\omega_0) & -\frac{1}{L_e}\mathbf{P}_{S3} \\ \frac{\mathbf{Q}_{S1}+\mathbf{Q}_{S2}}{C} & \frac{1}{C}\mathbf{Q}_{S1} & \frac{1}{C}\mathbf{Q}_{S3} & \mathbf{O}_3 \end{bmatrix}$$

and $\mathbf{U}_1$ is the unit matrix (123×123). $\mathbf{O}$, $\mathbf{O}_1$, $\mathbf{O}_2$, $\mathbf{O}_3$ and $\mathbf{O}_4$ are the zero matrices with dimensions (41×1), (41×123), (123×41), (41×41) and (123×123) respectively (a total of 20 harmonics are considered).

The solution of Eq. (38) gives complete information about the harmonics in the GUPFC, under steady and dynamic state conditions. The steady state solution of (38) can be obtained by setting $\dot{\mathbf{I}}_R(t)$, $\dot{\mathbf{I}}_S(t)$, $\dot{\mathbf{I}}_T(t)$ and $\dot{\mathbf{V}}_{dc}(t)$ to zero. Thus, the following algebraic equations represent the steady state

$$\begin{bmatrix} \mathbf{I}_R(t) \\ \mathbf{I}_S(t) \\ \mathbf{I}_T(t) \\ \mathbf{V}_{dc}(t) \end{bmatrix} = -\frac{\mathbf{G}_U{}^{-1}(t)}{L_e} \begin{bmatrix} \mathbf{U}_1 & -\mathbf{U}_1 & \mathbf{O}_4 & O_2 \\ -\mathbf{U}_1 & 2\mathbf{U}_1 & \mathbf{O}_4 & O_2 \\ \mathbf{O}_4 & -\mathbf{U}_1 & \mathbf{U}_1 & O_2 \\ O_1 & O_1 & O_1 & O_3 \end{bmatrix} \begin{bmatrix} \mathbf{V}_R(t) \\ \mathbf{V}_S(t) \\ \mathbf{V}_T(t) \\ O \end{bmatrix} \tag{39}$$

The solutions of the steady state equations (39) are used as the initial conditions for solving (38) provided, inverse of $\mathbf{G}_U(t)$ exists where the voltage $\mathbf{V}_{dc}(t)$ is a complex vector with harmonic coefficients given by

$$\mathbf{V}_{dc}(t) = [V_{dc_{-h}}(t) \cdots V_{dc_0}(t) \cdots V_{dc_h}(t)]^T$$

$\mathbf{I}_R(t)$, $\mathbf{I}_S(t)$ and $\mathbf{I}_T(t)$ are three-phase source currents. The representation of $\mathbf{I}_R(t)$ in the three phase frame of reference, takes the form,

$$\underbrace{\mathbf{I}_R(t)}_{123\times1} \Rightarrow \begin{bmatrix} \mathbf{I}_R^A(t) \\ \mathbf{I}_R^B(t) \\ \mathbf{I}_R^C(t) \end{bmatrix}; \mathbf{I}_R^A(t) = \underbrace{\begin{bmatrix} I_{R_{-h}}^A(t) \\ \vdots \\ I_{R_{-1}}^A(t) \\ I_{R_0}^A(t) \\ I_{SR}^A(t) \\ \vdots \\ I_{R_h}^A(t) \end{bmatrix}}_{41\times1}; \mathbf{I}_R^B(t) = \underbrace{\begin{bmatrix} I_{R_{-h}}^B(t) \\ \vdots \\ I_{R_{-1}}^B(t) \\ I_{R_0}^B(t) \\ I_{R_1}^B(t) \\ \vdots \\ I_{R_h}^B(t) \end{bmatrix}}_{41\times1}; \mathbf{I}_R^C(t) = \underbrace{\begin{bmatrix} I_{R_{-h}}^C(t) \\ \vdots \\ I_{R_{-1}}^C(t) \\ I_{R_0}^C(t) \\ I_{R_1}^C(t) \\ \vdots \\ I_{R_h}^C(t) \end{bmatrix}}_{41\times1}$$

$\mathbf{I}_S(t)$, $\mathbf{I}_S(t)$, $\mathbf{V}_R(t)$, $\mathbf{V}_S(t)$, and $\mathbf{V}_T(t)$ also take the same form as $\mathbf{I}_S(t)$. The size of each phase current and voltage is equal to $2h+1$. Total harmonics considered for the GUPFC case study is 20. The size of the DHD GUPFC system model equations that need to be solved is very large when more harmonics are considered. Factorization can be applied to the Jacobian since it is very sparse. The computing time of the

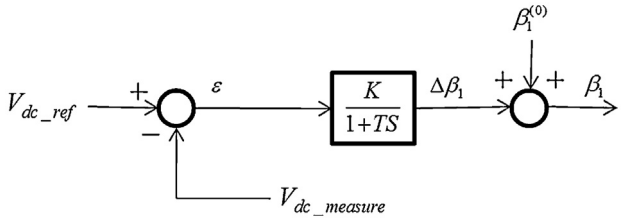

Fig. 3. Control system.

DHD model of the GUPFC can be significantly reduced if the highly sparse characteristic of the resulting matrices is taken into consideration and sparse-matrix techniques are used.

4. Numerical example

To illustrate the advantage of using the DHD model of the GUPFC (38) in the investigation of the dynamic response of harmonics to a given disturbances, a numerical example is considered. Under steady state conditions, the bus per-phase voltages of the GUPFC V_S, V_R, and V_T per unit at a frequency of 60 Hz, are

$$v_{Sa}(t) = 1.5 \sin \omega_0 t \quad v_{Sb}(t) = 1.5 \sin(\omega_0 t - 120^\circ) \quad v_{Sc}(t) = 1.5 \sin(\omega_0 t + 120^\circ)$$
$$v_{Ra}(t) = 1.6 \sin \omega_0 t \quad v_{Rb}(t) = 1.6 \sin(\omega_0 t - 120^\circ) \quad v_{Rc}(t) = 1.6 \sin(\omega_0 t + 120^\circ)$$
$$v_{Ta}(t) = 1.95 \sin \omega_0 t \quad v_{Tb}(t) = 1.95 \sin(\omega_0 t - 120^\circ) \quad v_{Tc}(t) = 1.95 \sin(\omega_0 t + 120^\circ)$$

This GUPFC model is simulated using PWM switching technique, whose function is calculated using the harmonic elimination method, to eliminate harmonics $i = 5, 7, 11, 13$, and 17. The magnitude of the fundamental of the inverter AC voltage can be adjusted by controlling the voltage across the capacitor. This can be achieved by changing the phase angle of the operation of the inverter switches with respect to the AC system [38]. In this case a phase angle of 15° is considered. The simulation starts at $t_0 = 0$ and ends at the final time of $t_f = 0.2$ s with an integration time step of $\triangle t = 0.2$ ms. It is assumed that voltage disturbances are happened twice during the entire simulation period. The first voltage disturbance occurs at 0.08 s and lasting for 5 ms, resulting in the reduction of the voltage on phase a by 50% of its given operating value at bus voltage V_T. The other voltage disturbance occurs at 0.13 s and lasting for 10 ms, resulting in the increase of the voltage on phase a by 50% of its given operating value at bus voltage V_T. For accuracy of the DHD method, a total of 20 harmonics are considered. The simulations are performed using MATLAB® software. The integration method used for these simulations is ode45 (), which is a fourth-order-Runge–Kutta algorithm that is built-in MATLAB® software.

For the proper operation of the GUPFC, it is necessary to keep the DC voltage as constant as possible during the steady and the disturbances periods. In order to show the usefulness of DHD model of the GUPFC, a feedback controller is designed using the DC side output, which helps in maintaining DC voltage constant during the simulation period.

4.1. PI control system for the GUPFC

The voltage across the capacitor can be controlled by varying, $\beta_1^{(0)}$, the phase angle of the inverter switches, with respect to the corresponding phase angle of the AC system voltage, to achieve the added advantage of being able to control the inverter output voltage [38]. The control system [16] shown in Fig. 3 is used to maintain the DC voltage across the capacitor, as constant as possible, in the simulation of the dynamic model of the GUPFC. Solving the GUPFC steady state eq. (39) yields the reference DC voltage of $V_{\text{dc\_ref}}$. A new phase angle, β_1, for the converter is calculated by adding the phase angle from control system $\Delta\beta_1$ to the steady state angle $\beta_1^{(0)}$. Now the new switching angle for the VSC 1 is calculated from β_1.

The following is the state-space equation for the control:

$$\frac{d\Delta\beta_1}{dt} = -\frac{1}{T}\Delta\beta_1 + \frac{K}{T}\varepsilon; \quad \varepsilon = V_{\text{dc\_ref}} - V_{\text{dc\_measure}}; \quad \beta_1 = \Delta\beta_1 + \beta_1^{(0)}$$

where $V_{\text{dc\_measure}}$ is the DC-term of the actual V_{dc}.

Fig. 4 shows the DC component of the DC side voltage with and without the control system during the steady state and disturbance interval. This Figure shows that, during the disturbance interval without the control system on DC side, the DC component of the voltage on the DC side drops and rises by 34% of its steady state value when the phase a voltage of V_T drops by 50% and rises by 50%, respectively. With the control system, the DC component of the voltage is very close to its steady state value during the two disturbances, thus indicating that the control system does indeed decrease the distortion during the disturbance. These results were obtained with a controller using a time constant (T) of 0.001 s and a gain (K) of 20. In the designing of this DC side control system, the accurate information of the DC-term of the $V_{\text{dc}}(V_{\text{dc\_ref}})$ at every time step is very important for keeping the DC side voltage constant.

As mentioned before, it is not possible to capture the accurate harmonic response of the system using time-domain with WFFT during fast disturbances, confirming that DHD models should be preferred.

The dynamic power quality indices are calculated to show the utilization of the proposed DHD model of the GUPFC in highlighting the sensitivity of the harmonic response of these devices to disturbances. From (19) it can be observed that harmonic coefficients are time dependent. This allows following step-by-step harmonic behavior along the transient with accuracy. However, the accuracy is dictated by number of harmonics considered.

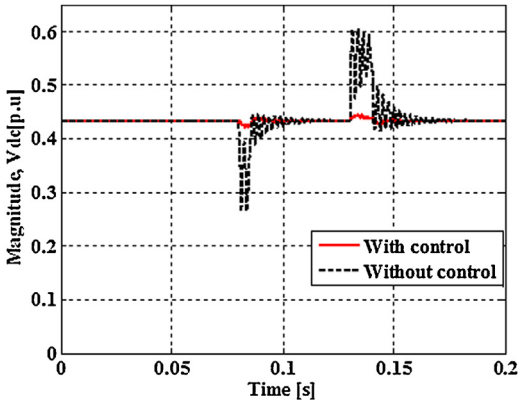

Fig. 4. DC-side voltage of GUPFC with and without control system.

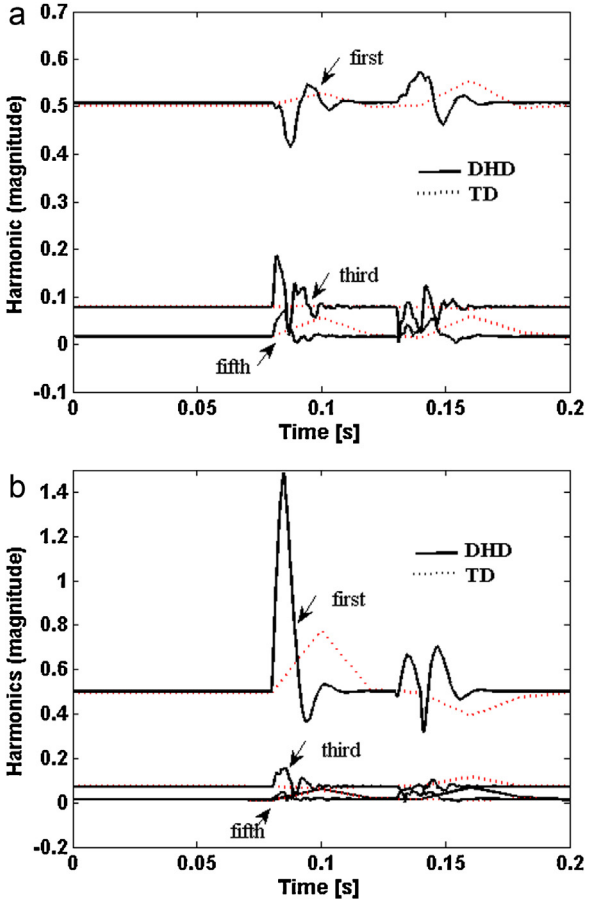

Fig. 5. (a) Harmonic content of output voltage of phase *a* of VSC 2. (b) Harmonic content of output voltage of phase *a* of VSC 3 (TD-WFFT in dotted line, DHD in continuous line).

The harmonic coefficients in the output voltages of the three voltage source converters $\mathbf{V}_R(t)$, $\mathbf{V}_S(t)$ and $\mathbf{V}_T(t)$, respectively are calculated using the harmonic coefficients $\mathbf{I}_R(t)$, $\mathbf{I}_S(t)$ and $\mathbf{I}_T(t)$ in (38). The harmonic content of the output voltage of phase *a* of VSC2 and VSC3 are plotted in Fig. 5(a) and (b). It shows harmonic content of output voltage of phase *a* of VSC 2 and VSC 3, including the fundamental, the third and the fifth harmonics (shown by continuous line, DHD). The drop and raise in the fundamental component of the phase *a* of VSC 2 is due to the decrease and increase in the DC side voltage during the disturbance intervals.

For comparison purposes, in Fig. 5(a) and (b), are also shown the time-domain variations of the same harmonics in voltages of phase a of VSC 2 and VSC 3. The dotted curves (TD) correspond to those obtained by the WFFT, based on 1200 data points and sliding window of 100 points width. In order to diminish the leakage error, each windowed data was multiplied by the data window by Von Hann.

From these results, it is observed that the WFFT (TD) follows the harmonic content obtained from DHD with some error, when compared with the precise values of the harmonic coefficients $\left[\, V_{-h}(t) \;\; \cdots \;\; V_{-1}(t) \;\; V_0(t) \;\; V_1(t) \;\; \cdots \;\; V_h(t) \,\right]$ in the output voltages of VSC2 and VSC3 given by the DHD model of the GUPFC. As expected, the error of the WFFT becomes smaller as the voltage waveforms straighten out

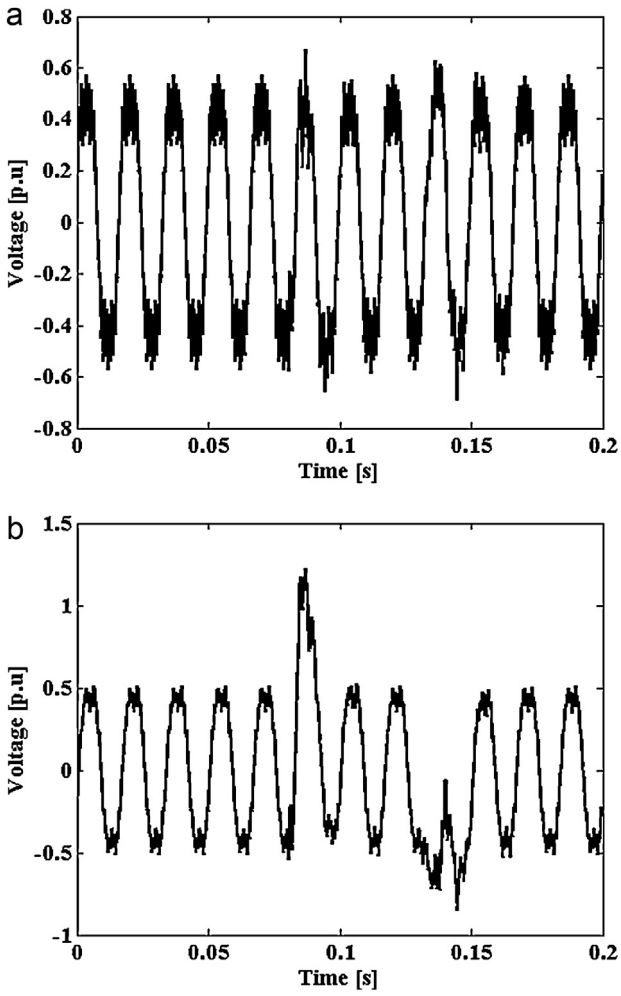

Fig. 6. (a) Time domain output voltage waveforms of phase *a* of VSC 2. (b) Time domain output voltage waveforms of phase *a* of VSC 3, obtained from the DHD simulation data.

to steady state. This can be observed from the harmonic content of the voltages presented in Fig. 5, and also that the accuracy of the DHD, particularly during the transient, is clearly superior to the one produced by the WFFT.

All the bus voltages in the circuit are connected at $t = 0$ and output voltages at VSC 2 and VSC 3 and their harmonic content are calculated by using the DHD equations with $h = 20$. The time domain voltage waveforms of VSC 2 and VSC 3, shown in Fig. 6, are derived by combining the harmonics, shown in Fig. 5 via(12). As expected, they exhibit more distortions during the disturbance interval than when in steady period.

4.2. Computing time

The computing time required to solve the GUPFC model by DHD and TD-WFFT are 13.2 and 7.3 s, respectively. The simulations were carried out using MATLAB® on a Pentium IV, 3-GHz, 2-GB RAM using a time step of 0.1667 ms. It can be observed from the Fig. 5 that the dynamics of the harmonics resulting from the TD-WFFT are not acceptable during the disturbance period. Especially during the fast disturbances, the harmonic information obtained from the DHD is far superior to TD-WFFT. But, the computational efficiency of the DHD is lower than the application of the TD-WFFT. However, the computing time of the DHD model of the GUPFC can be significantly reduced if the highly sparse characteristic of the resulting matrices is taken into consideration and sparse-matrix techniques are used.

4.3. Validation of the proposed DHD model of the GUPFC

The time domain solution of the GUPFC can be obtained by the following two methods Method 1 solving state space equations that describe the dynamics of the GUPFC, by a standard numerical integration method. Method 2 converting the harmonic information obtained from the DHD model into time domain.

The Fig. 7 shows the VSC 1, and VSC 2 output currents obtained from the above two methods. The time domain solutions obtained from Methods 1 and 2 are matching throughout the simulation period except at the beginning. It can be seen from Fig. 7 that solutions obtained from the TD and DHD did not match for the first 0.02 s and they matched after that. This is because obtaining steady-state solution for switching load is one of the essential features of DHD methodology. It has been reported that full initialization methods are not fully

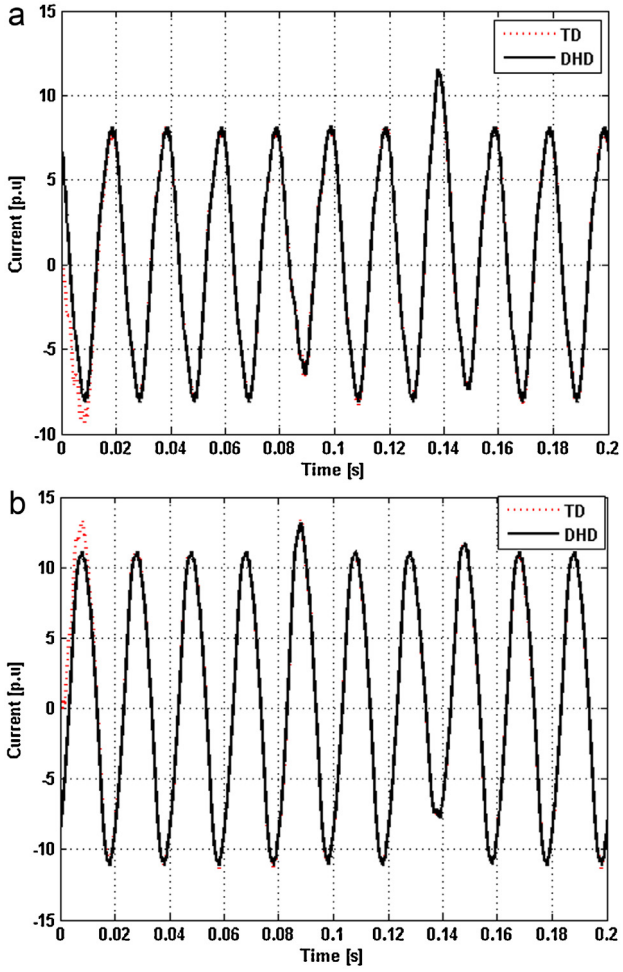

Fig. 7. (a) Comparison of time-domain results with Methods 1 and 2 for VSC1. (b) Comparison of time-domain results with Methods 1 and 2 for VSC2.

implemented in time domain methods [EMTP] [37]. This shows the effectiveness of using DHD technique in obtaining the steady-state solutions.

5. Conclusion

This paper presents the development of a DHD model for the GUPFC which provides for a unified solution to analyze its transient and steady state response to voltage disturbances. The advantage is that the proposed DHD model provides a direct means of calculating both the steady state values of the harmonics and the transient response of the harmonics to a disturbance. The transient and steady state responses are available from the explicit time-evolution of the harmonics that the method provides. The validation of the proposed DHD model of the GUPFC has been made through the original ODEs in the time domain. The results obtained from the dynamic behavior of the harmonics are valuable in the analysis of the stability and resonance of the system and in the analysis and design of control systems. However, designing a control system using the harmonic information is beyond the scope of this paper, and it is relegated to a future paper. The proposed methodology can be useful in validating FFT- based methods wherever it is applicable. Harmonic power flow in transmission lines and multi-line FACTS controllers is another area of future research.

References

[1] High-power electronics and flexible AC transmission systems, IEEE Power Engineering Review (1988), July 3–4.
[2] N.G. Hingorani, High-power electronics, Scientific American (November) (1993) 2–9.
[3] L. Gyugyi, Understanding FACTS: Concepts and Technology of Flexible AC Transmission Systems, IEEE Press, New York, 2000.
[4] G.C. Verghese, Nonlinear Phenomena in Power Electronics, IEEE Press, New York, 2001.
[5] A. Semlyen, N. Rajakovic, A harmonic domain computational package for nonlinear problems and its application to electric arcs, IEEE Transactions on Power Delivery 5 (July (3)) (1990) 1390–1397.
[6] J.A. Medina, Power Systems Modeling in Harmonic Domain, University of Canterbury, Christchurch, New Zealand, 1992 (PhD thesis).
[7] E. Acha, Modeling of Power System Transformers in the Complex Conjugate Harmonic Domain Space, University of Canterbury, Christchurch, New Zealand, 1988 (Ph.D. dissertation).
[8] N. Rajakovic, Harmonic domain modeling of laminated iron core, IEEE Transactions on Power Delivery 4 (January (1)) (1989) 382–390.
[9] M. Madrigal, Power Systems Harmonics, Computer Modeling and Analysis, Wiley, New York, 2001.
[10] P.S. Fjeld, C.C. Liu, D. Pierce, L. Tu, G. Hensley, Application of the windowed FFT to electrical power quality assessment, IEEE Transactions on Power Delivery 14 (October (4)) (1999) 1411–1416.
[11] B.C. Smith, N.R. Watson, J. Arillaga, Modeling of HVDC transmission systems in the harmonic domain, IEEE Transactions on Power Delivery 14 (July (3)) (1999) 1075–1080.

[12] N.R. Watson, Modeling of bipolar HVDC links in the harmonic domain, IEEE Transactions on Power Delivery 15 (July (3)) (2000) 1034–1038.
[13] C.S. Bruce, A Harmonic Domain Model for the Interaction of the HVdc Converter with AC and DC Systems, University of Canterbury, Christchurch, New Zealand, 1996 (Ph.D. dissertation).
[14] M. Madrigal, Modelling of Power Electronics Controllers for Harmonic Analysis in Power Systems, University of Glasgow, Glasgow, 2001 (Ph.D. dissertation).
[15] A. Semlyen, M.R. Iravani, Harmonic domain periodic steady-state modeling of power electronics apparatus: FC-TCR and TCSC, IEEE Transactions on Power Delivery 18 (July (3)) (2003) 960–967.
[16] M. Madrigal, B. Vyakaranam, R. Rarick, F.E. Villaseca, Dynamic companion harmonic circuit models for analysis of power systems with embedded power electronics devices, Electric Power Systems Research Journal 81 (February (2)) (2011) 340–346.
[17] E. Acha, T.J.E. Miller, Harmonic domain modeling of three phase thyristor-controlled reactors by means of switching vectors and discrete convolutions, IEEE Transactions on Power Delivery 9 (July) (1994) 1609–1615.
[18] E. Acha, Modelling of Custom Power Equipment using Harmonic Domain Techniques, in: Proceedings of the 9th International Conference on Harmonics and Quality of Power 1 (October), 2000, pp. 264–269.
[19] G.N. Bathurst, N.R. Waston, A.R. Wood, Harmonic domain approach to STATCOM modeling, IEE Proceedings on Generation, Transmission, Distribution 152 (March (2)) (2005) 194–200.
[20] N.R. Waston, A.R. Wood, Unbalanced SSSC modeling in the harmonic domain, in: Proceedings of the 7th International Power Engineering Conference 2 (November), 2005, pp. 705–710.
[21] C.D. Collins, FACTS device modeling in the harmonic domain, University Canterbury, New Zealand, 2006 (PhD dissertation).
[22] N.R. Waston, A.R. Wood, UPFC modeling in the harmonic domain, IEEE Transactions on Power Delivery 21 (April (2)) (2006) 933–938.
[23] M. Madrigal, E. Acha, Dynamic harmonic evolution using the extended harmonic domain, IEEE Transactions on Power Delivery 18 (April (2)) (2003) 587–594.
[24] M. Madrigal, J.J. Rico, Operational matrices for the analysis of periodic dynamic systems, IEEE Transactions on Power System 19 (August (3)) (2004) 1693–1695.
[25] B. Vyakaranam, M. Madrigal, F.E. Villaseca, R. Rarick, Dynamic harmonic evolution in FACTS via the extended harmonic domain method, in: Power and Energy Conference at University of Illinois, Urbana-Champaign, IL, February, 2010, pp. 29–38.
[26] B. Vyakaranam, Dynamic Harmonic Domain Modeling of Flexible Alternating Current Transmission System Controllers, in: Cleveland State University, OH, USA, 2011 (Doctoral dissertation).
[27] P. Zúñiga-Haro, Harmonic Modeling of Multi-Pulse SSSC, in: Power Tech, IEEE Bucharest, 2009, pp. 1–8.
[28] J.J. Chavez, A. Ramirez, V. Dinavahi, Dynamic harmonic domain modeling of synchronous machine and transmission line interface, Generation, Transmission & Distribution, IET 5 (9) (2011) 912–920.
[29] J.J. Chavez, A. Ramirez, Dynamic harmonic domain modeling of transients in three-phase transmission lines, IEEE Transactions on Power Delivery 23 (4) (2008) 2294–2301.
[30] A. Ramirez, The modified harmonic domain: interharmonics, IEEE Transactions on Power Delivery 26 (1) (2011) 235–241.
[31] M. Madrigal, J.J. Rico, Operational matrices for the analysis of periodic dynamic systems, IEEE Transactions on Power Systems 19 (3) (2004) 1693–1695.
[32] J. de Jesus Chavez, A modified dynamic harmonic domain distribution line model, IEEE Power and Energy Society General Meeting (2010) 1–7.
[33] B. Shperling, E. Uzunovic, S. Zelingher, Multi-Converter FACTS Devices: The Generalized Unified Power Flow Controller (GUPFC), in: IEEE 2000 PES Summer Meeting, Seattle, USA, July, 2000.
[34] A.M. Stankovic, T. Aydin, Analysis of asymmetrical faults in power systems using dynamic phasors, IEEE Transactions on Power Systems 15 (August (3)) (2000) 1062–1068.
[35] N.M. Wereley, Linear time periodic systems: transfer function, poles, transmission zeros and directional properties, American Control Conference (June) (1991) 1179–1184.
[36] J.M. Noworolski, X.Z. Lui, G.C. Verghese, Generalized averaging method for power conversion circuits, IEEE Transactions on Power Electronics 6 (April (2)) (1991) 251–259.
[37] J.A. Martinez, Power Quality Analysis using Electromagnetic Transient Programs, in: Proceedings of the ICHQP-98, Athens, Greece, October, 1998, pp. 590–597.
[38] W.T. Norris, Exact analysis of a multi-pulse shunt converter compensator or Statcon. I. Performance, IEE Proceedings-Generation, Transmission and Distribution 144 (March (2)) (1997) 213–218.
[39] P. Mattavelli, G.C. Verghese, A.M. Stanković, Phasor dynamics of thyristor-controlled series capacitor systems, IEEE Transactions on Power Systems 12 (1997) 1259–1267.
[40] P. Mattavelli, V. Caliskan, G.C. Verghese, Modeling and analysis of FACTS devices with dynamic phasors, IEEE Power Engineering Society Winter Meeting (2000) 1440–1446.